Origin of the crossover between a freezing and a structural transition at low concentration in the relaxor ferroelectric $K_{1-x}Li_{x}TaO_{3}$

Ling Cai, Jean Toulouse, Leland Harriger, R. Gregory Downing, and L. A. Boatner

Phys. Rev. B **91**, 134106 — Published 16 April 2015

DOI: 10.1103/PhysRevB.91.134106

Origin of the cross-over from a freezing to a structural transition in the relaxor ferroelectric $K_{1-x}Li_xTaO_3$

Ling Cai,[1,*] Jean Toulouse,[1] Leland Harriger,[2] R. Gregory Downing,[2] and L.A. Boatner[3]

[1] *Physics Department, Lehigh University, Bethlehem, PA, 18015*

[2] *NIST Center for Neutron Research, National Institute of Standards and Technology, Gaithersburg, MD,20899*

[3] *Center for Radiation Detection Materials and Systems, Oak Ridge National Laboratory, Oak Ridge, TN, 37831*

The origin of the relaxor behavior in $K_{1-x}Li_xTaO_3$(KLT) and other disordered perovskites is now recognized to be due to the reorientation of the polar nanodomains (PNDs) formed by the correlated dipoles of off-center ions. The collective dynamics of these systems evolve through several temperature stages. On decreasing temperature below the so-called Burns temperature T_B, individual dipoles become correlated within nano-size regions. On further cooling, the slow dynamics of these polar regions allow local lattice distortions to take place and formation of polar nanodomains at $T^* < T_B$. At still lower temperature, some relaxors undergo a phase transition while others do not. In KLT, there is a critical Li concentration $x_c = 0.022$ above which the system undergoes a structural transition at T_c, and below which it freezes in a dipole glass state at T_f. To better understand the nature of this critical concentration, the changes that occur upon crossing it and the nature of the dipole glass sate, the collective dynamics of KLT have been studied by dielectric spectroscopy and neutron diffraction for two Li concentrations ($x = 0.026$ and 0.018), close to but straddling the critical concentration x_c. Two very different transitional behaviors are observed. Just below this critical concentration, KLT displays critical slowing down and the onset of freezing as seen in hydrogen bonded molecular ferroelectrics, while just above this concentration, KLT undergoes a first order structural transition.

PACS numbers: 77.80.Jk, 77.22.Gm, 25.40.Dn, 64.70.K-

I. INTRODUCTION

As a prototypical A-site disordered relaxor ferroelectric, $K_{1-x}Li_xTaO_3$ (KLT) has been a useful model system for answering some of the outstanding questions concerning the behavior of relaxors and its evolution with temperature. In KLT, as a result of the size mismatch between Li and K, the substituted Li cations are displaced from their normal cubic A-site positions off-center by ~ 1.2 Å in a cubic direction [1]. This off-centering gives rise to dipole moments that can reorient in an applied electric field, resulting in the characteristic frequency dispersion of the dielectric permittivity of relaxors. Two modes of dipole relaxation are observed in KLT, a $\pi/2$ relaxation and a π relaxation, corresponding respectively to a 90° and a 180° flip of the Li dipoles between cubic directions [2]. Because of its lower thermal activation energy, the $\pi/2$ relaxation takes place at a lower temperature than the π relaxation. At lower temperatures, the Li dipoles become correlated and reorient collectively within polar nanodomains (PNDs). As a result, the strength of the relaxations increases non-linearly with Li concentration. Although the $\pi/2$ relaxation is the dominant mode for low Li concentrations, the strength of the π relaxation increases faster with increasing Li concentration ($x > 0.05$). In the present study we are primarily concerned with the $\pi/2$ relaxation since the changes of interest in transitional behavior occur in the lower Li concentration regime and at temperatures just below the $\pi/2$ relaxation.

In a study of KLT over a wide range of Li concentrations, Kleemann *et al.* identified a cross-over concentration in the range $0.016 < x < 0.026$, or at an extrapolated value $x_c \sim 0.022$ [3]. For $x < x_c$, the system remains macroscopically cubic, although it still displays the relaxor behavior and has been characterized as being in a dipole glass state of randomly oriented frozen dipoles. For $x > x_c$, long range tetragonal order develops, which manifests itself as a sharp drop in dielectric permittivity, the more pronounced the lower the frequency [4,5]. Yet, no macroscopic switchable polar order is observed if cooled in zero field [6,7]. For $x > x_c$, KLT is therefore structurally ordered but not ferroelectric at low temperature [7]. The present study has focused more narrowly on the nature of this critical concentration and on the changes in collective dynamics taking place on either side of it.

For pure $KTaO_3$, the zero point fluctuations prevent the occurrence of a phase transition down to the lowest temperature. It has therefore been labeled as quantum paraelectric. The addition of lithium breaks the symmetry locally and induces a transition, local below a critical concentration and macroscopic above. At extremely low Li concentrations, KLT exhibits a so-called chiral glass state in which the dipole impurities can be regarded as non-interacting [8]. Other studies have reported that, in the low concentration regime, KLT displays a combination of glassy and ferroelectric properties [9,10]. Although it does not undergo a long range structural transformation on cooling, low concentration KLT displays a slowing down of the dipolar relaxation which eventually leads to the freezing of randomly oriented dipoles, i.e. it falls out of thermodynamic equilibrium. This behavior in relaxor systems can be described as ergodicity-breaking [11]. Near the critical concentration, x_c, KLT offers a special oppor-

tunity to study the evolution of the transitional behavior of a relaxor as a function of composition, from what is akin to a glass transition to a structural transition. KLT and other relaxors are in an ergodic state as long as the correlated dipoles within PNDs can relax/reorient so that the system is able to reach thermodynamic equilibrium at a given temperature and in a given external field. Ergodicity-breaking occurs at low temperatures when the relaxation dynamics slow down to either an arrest or to such a point that the relaxation time exceeds the experimental time and the system can no longer reach an equilibrium distribution of the dipoles. As a result, the ensemble average for an observable of the system is no longer equal to its time average. Ergodicity-breaking can therefore be categorized into two classes: i) discontinuous with a sudden loss of entropy, reflecting collective behavior (*e.g.* as in the freezing of supercooled glass-forming liquids) [12] or ii) continuous with progressively greater loss of entropy due to the limits of the experimental time or frequency (*e.g.* as in slowly cooled glass-forming liquids) [13]. The first type of ergodicity-breaking is due to an actual loss of degrees of freedom while the second type is only due to a decrease in the number of microstates that are accessible by the system on the experimental time scale. The latter should therefore vary with measurement techniques that have different characteristic time scales or with frequency if measured as a function of frequency.

In the present study, we have used neutron diffraction and dielectric spectroscopy to characterize the structure and follow the polar dynamics with temperature of two KLT crystals with relatively close Li concentrations, x=0.026 and x=0.018, lying on opposite sides of the critical concentration, $x_c \approx 0.022$. Despite this small concentration difference, the dielectric spectroscopy and neutron diffraction results reported below reveal very different transitional behaviors. The higher concentration KLT crystal undergoes an equilibrium first order structural transition while the lower concentration one exhibits an ergodic to non-ergodic transition akin to the glass/jamming transition observed in glasses and granular materials [14]. The change in transitional behavior is therefore quite abrupt on crossing over the critical concentration.

II. EXPERIMENTAL DETAILS

Two transparent single crystal KLT samples, KLT1.8 and KLT2.6 were grown by slow cooling method from solution at Oak Ridge National Lab. The two crystals were cut along (100) faces. KLT1.8 had dimensions of $\sim 7\times4\times3$ mm, and KLT2.6 dimensions of $\sim 8\times7\times4$ mm. The two samples were first characterized by dielectric spectroscopy at Lehigh and then taken to NIST Center for Neutron Research(NCNR) for neutron measurements.

For the dielectric measurements, metallic electrodes were evaporated on the two largest parallel surfaces of the samples. In order to rule out possible electrode-sample interface effects, different coating/interface conditions such as sputtered gold, aluminum vapor deposition and silver paint, were tested to ensure that the same dielectric results were obtained. Different polishing quality of the surfaces were also used, from rough to optical grade, and the same dielectric results were obtained in all cases. The sample was held stress-free inside an open cycle cryostat. The parallel plate capacitance and the loss tangent were measured with an impedance analyzer, sweeping the frequency from 100 Hz to 10 MHz. The measured capacitance was converted to a dielectric constant through the relation $\epsilon = Cd/A\epsilon_0$ where C is the capacitance, d the sample thickness, A the area of the electrode and ϵ_0 the free space permittivity. The samples were cooled with liquid helium from room temperature to ∼20 K. Cooling rate was controlled at an average rate of 0.2K/min and the temperature was stabilized at each temperature, allowing sufficient time for thermal equilibrium to be established before measurement.

The neutron experiments were performed at NCNR on the NG1 spectrometer for neutron depth profiling (NDP) measurement and on the SPINS spectrometer for the diffraction measurements. Both spectrometers use cold neutrons. For the diffraction measurements, the samples were mounted inside an evacuated aluminum canister and a closed cycle refrigerator (CCR) was used to cool the sample from room temperature to ∼10 K. The samples were aligned in the $[hk0]$ scattering plane and the pseudocubic notation was used throughout the measurements. The neutron final energy was fixed at E_f=5 meV, Beryllium filters were used before and after the sample to eliminate higher order contamination. Tight collimations of 20′-sample-20′ were also chosen in order to achieve the highest possible Q resolution. As a consequence, the diffraction scans were limited to the (100) and (110) Bragg reflections. Both dielectric and neutron measurements were performed on exact same KLT1.8 and KLT2.6 crystals. Nevertheless, due to difference in sample environment, differences of a few degrees in transition temperatures were observed between the two types of measurements. However, these are not consequential for the present study of the origin of the cross-over.

III. EXPERIMENT RESULT AND ANALYSIS

A. Neutron depth profiling and diffraction

The lithium concentrations of the two samples were verified before measuring their physical properties. Neutron depth profiling (NDP) was used to precisely determine the concentration of ^7Li (92.4% natural abundance) in the bulk. The relative concentrations of the two samples are shown in Fig. 1 (a) as a function of depth from the surface expressed in terms of channel numbers. The two different regions visible in the figure correspond to different particle reactions; the flat region at higher chan-

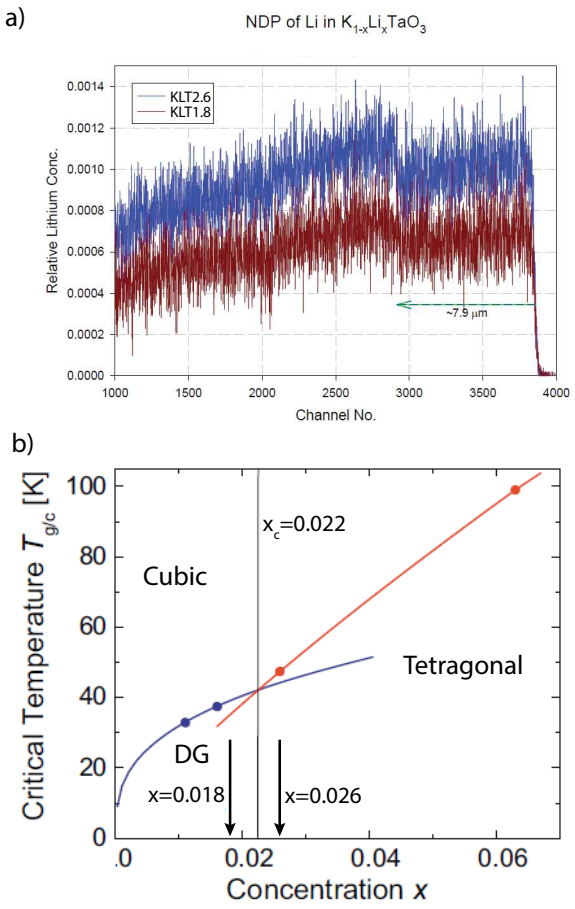

FIG. 1. (color online) (a) Neutron depth profiling measurement. (b) KLT phase diagram from dielectric measurements [8]. The arrows indicate the *Li* concentrations in the two samples investigated in the present study.

nel numbers, for depths of about 8 μm, corresponds to a tritium reaction while the sloped region at lower channel numbers corresponds to an alpha particle reaction. Concentrations of the relevant elements (here *Li*) can be obtained from a measure of the stopping power of the sample matter as a function of depth. References [15] and [16] provide a more complete description of the technique. Integrating the intensities from all channels, the overall ratio of the respective lithium concentrations in the two crystals was found to be 0.67. Using the observed transition temperature of the higher concentration crystal and the published phase diagram obtained from previous dielectric measurements [6,8], its lithium content was estimated to be 2.6%. Then using the experimentally determined ratio of the concentrations in the two crystals, the lithium content of the lower concentration crystal was calculated to be 1.8%, a concentration that is in good agreement with that obtained directly from the phase diagram. As shown by arrows in Fig. 1 (b), these concentrations lie just above and just below the estimated critical concentration $x_c \approx 0.022$.

To detect a possible structural transition in either one of the two KLT crystals investigated, neutron diffraction measurements were performed on a cold neutron triple axis spectrometer. Since the structural properties above and below the transition have been well studied previously [17–19], we only highlight the differences between the two samples without delving into details of the temperature dependence of the lattice parameters or unit cell volume. Fig. 2 (a) and (b) show the (100) Bragg reflections of KLT1.8 and KLT2.6 at temperatures above, near, and below a possible transition. The difference in the shapes of the Bragg peaks of the two samples is manifest. For the KLT2.6 crystal, a single symmetric peak is observed above the transition, which becomes distorted below. At T=40 K and 26 K, the Bragg peak can be satisfactorily fitted with two Gaussian functions shown by the solid gray lines in Fig. 2 (b), thus revealing a phase transition. By contrast, the corresponding Bragg peak for KLT1.8 retains the same symmetric shape at all temperatures as seen in Fig. 2 (a). Note that under the tight collimation conditions used, the Q resolution of the spectrometer of $\sim$0.005 r.l.u. would correspond to a change in the lattice constant of $\sim$0.012 $\AA$. Since the reported tetragonal distortion in KLT is less than that [17], a fully resolved peak splitting is not expected here. In conclusion, the strongly distorted Bragg peaks shown in Fig. 2 (b) for KLT2.6 are sufficient to confirm the occurrence of a (tetragonal) transition while the single symmetric peak observed in KLT1.8 at all temperatures indicates the absence of such a transition.

In the course of the diffraction measurements, we also measured the Bragg peak intensity as a function of temperature upon cooling and warming. For a single crystal with a small mosaicity, a structural phase transition is marked by a sudden change in intensity due to the strains associated with the transformation, the so-called relief of extinction effect. As shown in Fig. 2 (c), the KLT1.8 and KLT2.6 crystals indeed show an increase in intensity at $\sim$48 K and $\sim$51 K respectively. The Bragg intensity curves reveal a thermal hysteresis indicative of a metastability region within which the cubic and tetragonal phases can coexist [20,21]. It is important to note that the Bragg intensity of the KLT2.6 crystal in Fig. 2 (c) has been scaled down by a factor of 4, so that the actual extinction effect is more than four times stronger in KLT2.6 than in KLT1.8. Since no structural transformation to a long range tetragonal order takes place in the KLT1.8 crystal, the smaller relief of extinction in this crystal can only be attributed to the orientational freezing of the PNDs and their local strain fields. A similar observation was made by Wen *et al.* in a 2% KLT sample [22], who attributed the relief of extinction to the appearance of crystalline imperfections.

B. Dielectric permittivity

The real (ϵ') and imaginary (ϵ'') parts of the dielectric permittivity of the two samples are presented respectively in the top and bottom parts of Fig. 3. Both samples dis-

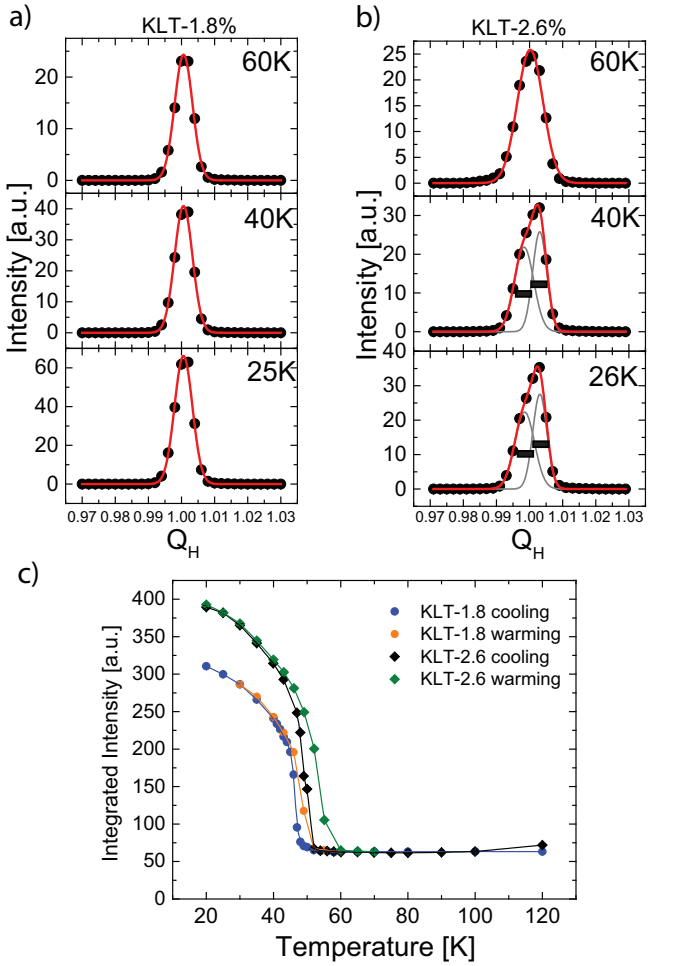

FIG. 2. (color online) (010) Bragg reflection measured at three temperatures for (a) KLT1.8 and (b) KLT2.6. The integrated intensity on cooling and warming are shown in (c). The horizontal bars in (b) indicate the instrumental resolution. The intensities for KLT2.6 in (c) are scaled down by a factor of 4.

play the strong relaxor behavior, with the $\pi/2$ relaxation being the dominant relaxation mode. The weak π relaxation can be seen near 80 K in Fig. 3 (a) and near 90 K in (b). As seen in Fig. 3 (b), the KLT2.6 crystal undergoes a transition that is clearly identifiable by the sharp drop of both parts of the dielectric permittivity at $T_c \sim 45$ K. It is worth noting that, because of the frequency dispersion of the $\pi/2$ relaxation peak, the magnitude of this drop is greater at lower frequencies and is more clearly seen in ϵ''. By contrast, KLT1.8 in Fig. 3 (a) exhibits a very different critical behavior which is characterized by a minimum (or saddle point) in the dielectric permittivity at $T_{min} \sim 44$ K. Most significant, the minimum appears at the same temperature for all frequencies, indicative of a critical phenomenon. This minimum results in a two peak feature, the two peaks merging with each other at lower frequencies, such that only a single peak is seen below 500 Hz. Comparing the sharp drop in permittivity at the transition in KLT2.6 and the minimum followed by residual dispersion in KLT1.8 points to two qualitatively different types of transition. The latter is reminiscent of the order-disorder transitions that are observed in hydrogen-bonded molecular ferroelectric systems, in which the transition is also marked by a minimum of the permittivity attributed to critical slowing down of molecular reorientations. [23–26].

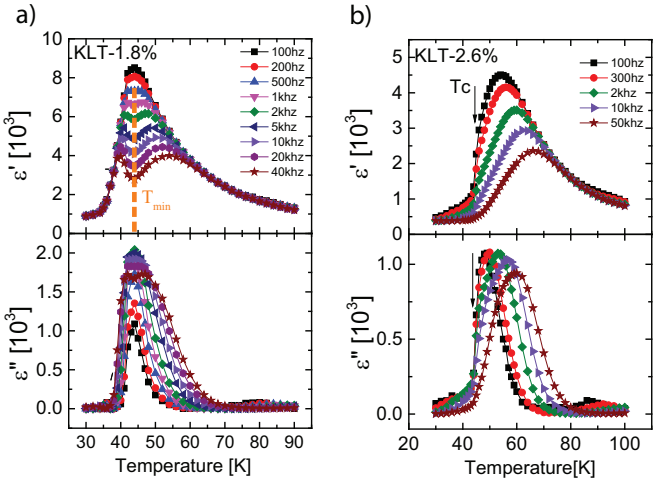

FIG. 3. (color online)Real and imaginary part of the dielectric constant of (a) KLT1.8 and (b) KLT2.6. The arrows indicate the glass freezing temperature T_f and phase transition temperature T_c respectively; the yellow dashed line indicates the temperature, T_{min}, of the minimum for KLT1.8.

The characteristic time of a relaxation process can be obtained from the relationship $\omega\tau_{mean}$=1 at the peak of the imaginary part of the permittivity, ϵ''. The frequency spectrum of the imaginary part of the dielectric constant is presented in Fig. 4 (a) and (c) for KLT1.8 and KLT2.6 respectively. The dielectric peaks are broad and possibly composed of two components. However, in the present study we did not distinguish between two separate components. In the case of the KLT1.8 crystal, the dielectric peak initially shifts to lower frequencies and increases in magnitude with decreasing temperatures, then reverts course without any discontinuity and begins shifting back towards higher frequencies, although decreasing in magnitude with further decrease of temperature. The turnaround temperature corresponds to the position of the minimum in Fig. 3 (a). In the case of KLT2.6, the dielectric peak also shifts to lower frequencies with decreasing temperatures down to the transition which is marked by a sudden drop in the magnitude of the peak at T_c. Using the $\omega\tau_{mean}$=1 relationship, a mean relaxation time, τ_{mean}, is obtained from the actual position of the ϵ'' peak for both crystals. τ_{mean} is plotted in Fig. 4 (b) and (d) for KLT1.8 and KLT2.6 respectively. The lines are fits to Arrhenius and Vogel-Fulcher laws with activation energies, $\delta U_{\pi/2} \sim 1250$ K and $\delta U_{\pi} \sim 2400$ K (π relaxation fit not shown in this figure) for both crystals, energies that are in good agreement with those from earlier studies [2,27,28]. To investigate the glassy behavior in the lower

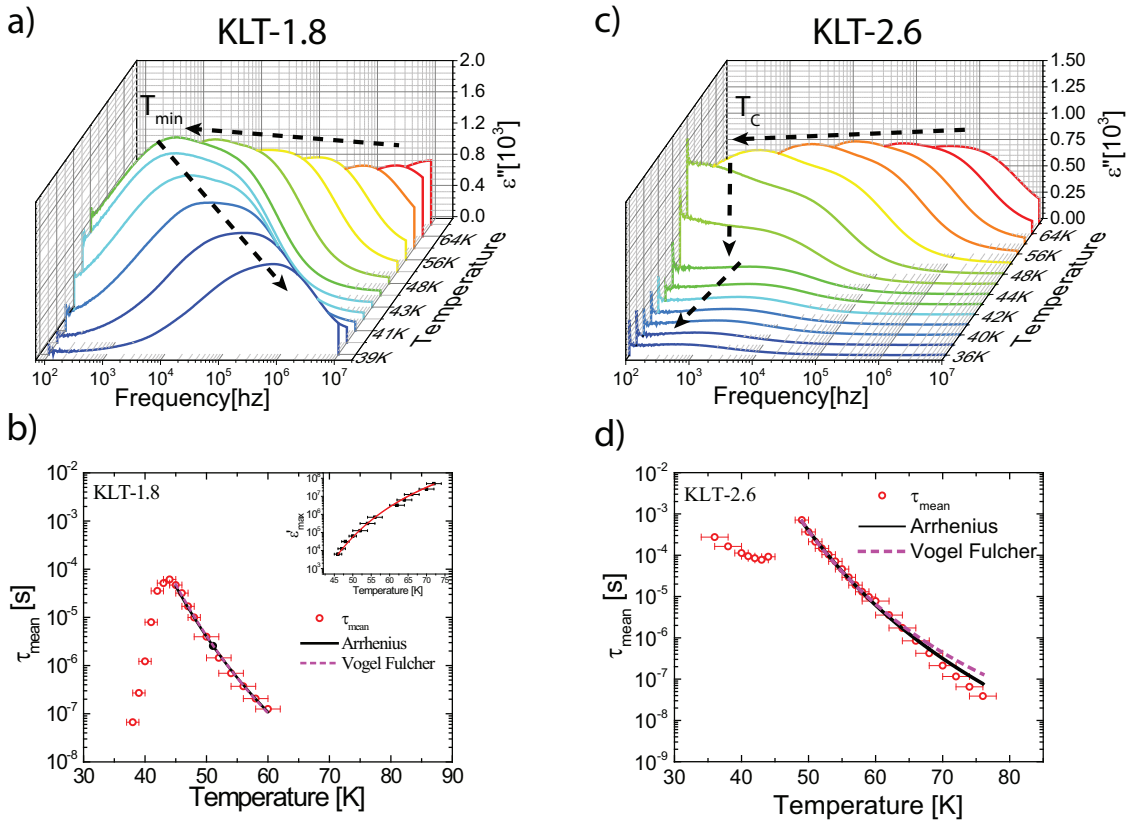

FIG. 4. (color online)Frequency spectra of imaginary part of the dielectric permittivity and mean relaxation time for KLT1.8 in (a) and (b), and for KLT2.6 in (c) and (d). The dashed lines in (a) and (c) are guides to the eye for the peak positions. The experimental curves for the relaxation times in (b) and (d) were fitted with both an Arrhenius and a Vogel-Fulcher law. The inset in (b) shows the fitting of VF law to the maxima of ϵ'

concentration crystal, the frequency maximum of its real part is plotted in the inset in Fig. 4 (b) and fitted to a Volgel-Fulcher law:

$$\omega = \omega_0 \, e^{-E/(T_{max}-T_{VF})} \qquad (1)$$

where ω_0 is a constant, E an activation energy and T_{VF} a freezing temperature. The fitting predicts a freezing temperature T_{VF}=12.7 K. This value agrees with that found by Yokota *et al.* on a KLT crystal with a similar concentration [10]. The present result indicates that T_{min} in KLT1.8 lies well above the global freezing temperature, T_{VF}, which suggests that strain plays an important part in the freezing process. The respective relaxation properties of the two KLT crystals studied can therefore be summarized as follows: i) in KLT1.8 the relaxation time reaches a finite upper limit (non-divergent critical slowing down) at T_{min} and decreases below this temperature, and ii) the relaxation time in KLT2.6 exhibits a discontinuity at T_c (structural transition) and then continues to increase below, albeit more slowly. It is important to emphasize that, even though the $\pi/2$ relaxation is not discontinuous in KLT1.8, its magnitude nevertheless decreases below T_{min}, indicating that a decreasing number of PNDs contribute with further decreasing temperature.

It is worth pointing out that the double peak structure in Fig. 3 (a) persists down to lower frequencies for ϵ' (down to 500 Hz) than for ϵ'' (down to 2 kHz). This is due to the fact that, when writing separately the real and imaginary parts of the permittivity, the expression for ϵ'' contains $\omega\tau$ in the numerator as $(\omega\tau\,\delta\epsilon)/(1+\omega^2\tau^2)$ while that for ϵ' does not. As a result, the decrease in τ_{mean} tends to lower both the numerator and denominator of ϵ'' such that the minimum is replaced by a peak at lower frequencies for ϵ'' than for ϵ', both are found at the same temperature T_{min}. Note that the frequency dispersion of the permittivity disappears for temperatures below the lower maximum for both the real and imaginary parts of the permittivity. This is due to the fact that the influence of the decreasing $\delta\epsilon$ becomes dominant over the influence of the decreasing τ_{mean}.

We now address the issue of the dielectric peak width and the distribution of relaxation times it reflects. The existence of a distribution of relaxation times which increases upon cooling has been recognized before [2,29,30]. It is a reflection of the random distribution of the dipoles and of the varying rates at which different PNDs grow upon cooling. Following Cole *et al.* [31], the distribution of relaxation times can be taken into account phenomenologically through a modification of the Debye expressions for the dielectric permittivity:

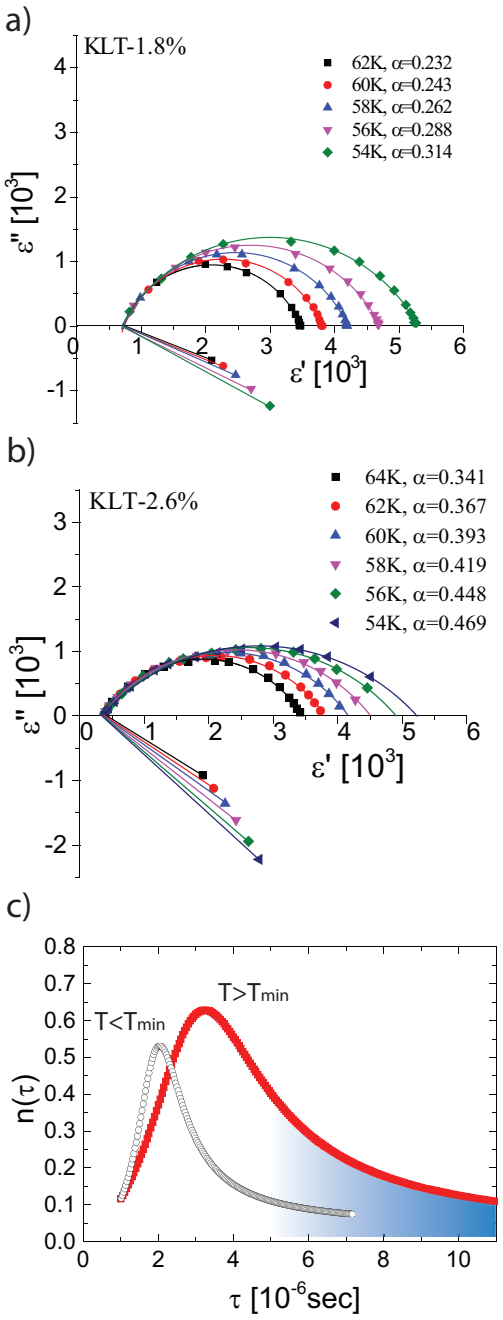

FIG. 5. (color online) Cole-Cole semicircle plot in the thermal equilibrium region in a) KLT-1.8 and b) KLT-2.6 respectively with α value given in the legend. The change in the relaxation time distribution function from equilibrium state(red square) to non-equilibrium state(black circle) are schematically plotted in c).

$$\epsilon^*(\omega) = \frac{\epsilon_s}{1 + (i\omega\tau_{mean})^{1-\alpha}} + \epsilon_\infty, \qquad (2)$$

known as the Cole function. In this equation, ϵ_s and ϵ_∞ are respectively the static (zero frequency) and high frequency dielectric constants, τ_{mean} is the mean relaxation time and $0 \leq \alpha \leq 1$ is a measure of the dispersivity of the relaxation or width of the distribution of relaxation times. Relative to the relaxation, the system is said to be monodispersive if $\alpha = 0$ and polydispersive if α is close to 1. The imaginary part of the permittivity can be similarly expressed in terms of these parameters. Plotting ϵ'' vs ϵ' (Cole-Cole plot), the Cole function traces a semicircle whose center lies on a straight line from the origin making an angle with the horizontal axis that is proportional to α. Fig. 5 (a) and (b) show the *Cole-Cole* semicircle plots for different temperatures above the transition. On each semicircle, the value of the high frequency dielectric constant, ϵ_∞, is found at the left intersection of the semi-circle with the horizontal axis and the static dielectric constant at the right intersection. As should be expected, the high frequency dielectric constant, ϵ_∞, is temperature independent while the static dielectric constant, ϵ_s, is strongly dependent on temperature. The semi-circles are found to be depressed for both crystals but, as indicated by the α values shown in the figure, more so for KLT2.6. Hence, KLT2.6 is more polydispersive than KLT1.8, which is not unexpected since the former crystal, with a higher *Li* concentration, contains both relatively independent/isolated dipoles as well as closely spaced and highly correlated dipoles within PNDs. The value of α increases with decreasing temperature for both crystals, indicating an increase in the dispersivity of the relaxation or increasing width of the distribution of relaxationtimes at lower temperatures, although smaller for KLT2.6.

IV. DISCUSSION

The dielectric results presented above show that both KLT2.6 and KLT1.8 display the relaxor behavior, indicating the presence of polar nanodomains in both. Yet, the interactions between these PNDs result in two qualitatively different transition behaviors. The temperature evolution of the Bragg peaks, on the one hand, and of the dielectric permittivity, on the other, provide complementary information on their different behaviors. KLT2.6 undergoes a symmetry lowering transition (cubic-tetragonal) which is revealed by the partial splitting of the [100] Bragg peak and a 30X increase of its magnitude due to a relief of extinction. By contrast, no similar transition is observed in KLT1.8 for which the Bragg peaks remain single and unchanged in shape, although a 5-6X relief-of-extinction increase in the intensity of its Bragg peaks is nevertheless observed between 45K and 50K. As a measure of the magnitude of the distortion at the phase transition, these respective relief of extinction figures reveal a 5 to 6 times larger distortion in KLT2.6 than in KLT1.8. The transformation in KLT1.8, which does not result in a macroscopic symmetry change, must therefore only be local or short range and can be described as a freezing transition.

The large symmetry change in KLT2.6 is also reflected in the dielectric behavior by a sharp drop of both the

real and imaginary parts of the permittivity at $T_c \approx 45\,\mathrm{K}$ while, in KLT1.8, they simply go through a transition-like minimum at higher frequencies and a single maximum at lower frequencies, all at the same temperature of $\sim 44\,\mathrm{K}$. In this lower concentration crystal, the peak on the high temperature side of the minimum exhibits the relaxor behavior. As the frequency is lowered, the dielectric measurements probe slower dynamics or dynamics corresponding to a longer relaxation time τ_{mean} and the relaxor peak therefore moves to lower temperatures, according to the $\omega\tau = 1$ condition, which strictly applies to the imaginary part, ϵ''. However, as shown by the results in Fig. 3 (a), the position of maximum of ϵ'' becomes pinned at the transition temperature for frequencies below 2 kHz and τ_{mean} no longer reaches this condition below the transition but instead decreases, as seen in Fig. 4 (b). Note that the maximum value of τ_{mean} in that figure corresponds indeed to 2 kHz.

As was pointed out in the Introduction, two different types of freezing can be distinguished, i) discontinuous or abrupt and ii) continuous or progressive. The observation of a non-divergent mean relaxation time τ_{mean} at T_{min} in KLT1.8 might seem to suggest that the observed freezing is continuous, even though the dielectric permittivity is seen in Fig. 3 (a) to go through a minimum at the same T_{min} for all frequencies, as in a transition. To understand this apparent contradiction, it is important to note that, while the relaxation time changes continuously with temperature, reaching a maximum at T_{min} and decreasing below, the magnitude of the relaxation peak also begins to decrease below T_{min}. Thus, a fraction of the previously relaxing PNDs collectively freezes at T_{min}, those with the longest relaxation times in the distribution. Because the minimum is observed at the same temperature for all frequencies, it corresponds to the sudden loss of a certain number of degrees of freedom of the system, i.e. a collective freezing transition. Smaller PNDs or isolated dipoles with shorter relaxation times nevertheless continue to relax and contribute to the dielectric permittivity below T_{min}, although fewer and fewer as they too progressively freeze with further decrease of temperature. This is schematically illustrated in Fig. 5 (c) which shows the position of the maximum of the distribution or τ_{mean} shifting toward shorter times with decreasing temperature below T_{min} while the magnitude of the peak is reduced. This evolution of the distribution explains the evolution of the permittivity in Fig. 4, which is the result of a competition between the number of relaxing PNDs or equivalently the relaxation strength, $\delta\epsilon \equiv \epsilon_s - \epsilon_\infty$, in the numerator of Eq. 2 and the relaxation time, τ_{mean}, in the denominator. For higher frequencies below T_{min}, the shorter τ_{mean} of the remaining dynamic PNDs or dipoles initially favors an increase of the permittivity but, with a continued reduction in the number of dynamic dipoles, the permittivity eventually decreases again at lower temperatures. The freezing transition in KLT1.8 is reminiscent of the glass/jamming transitions that are observed in glasses and granular materials [32,33]. It is a hybrid between a first and a second order transition in a disordered system, with the sudden freezing or lock-in of a subset of the dipoles or PNDs at the onset, followed by the progressive freezing or lock-in of the remaining ones with decreasing temperature.

In KLT2.6 by contrast, the first order structural transition to a tetragonal phase takes place throughout the crystal. The fact that the dielectric permittivity decreases abruptly at T_c and the absence of a switchable remnant polarization below the transition indicate that the PNDs are locked in their orientation in the tetragonal phase. As seen in Fig. 4 (c), the number of the remaining relaxing dipoles or the relaxation strength is very small below T_c. Although we have not measured the tetragonal distortion (c/a) as a function of temperature, the continued increase of the relaxation time τ below T_c can be attributed to the increasing distortion below the structural phase transition (see large relief of extinction in Fig. 2 (c)), making the relaxation of the few remaining isolated dipoles more and more difficult. In summary, while PNDs are present in both crystals, the main difference in their transition behaviors is the spatial extent of the structural transformation, uniform throughout the crystal for KLT2.6 but remaining local or medium range for KLT1.8. It is worthwhile to reiterate that the PNDs are intrinsically piezoelectric [20] and that their polarization generates a strain of the surrounding lattice. For a macroscopic structural transformation to take place, a critical level of strain and therefore local polarization is needed. In KLT2.6 the strain-driven transformation percolates throughout the entire crystal while, in KLT1.8, it remains medium range. The structural transition is facilitated by the fact that strain is an axial tensor, such that PNDs with their polarization pointing in opposite directions will drive the same structural distortion. The relatively abrupt cross-over in transition behavior observed across the critical concentration at $x_c = 0.022$ can thus be considered as the concentration at which strain percolates through the system.

Finally, in order to better understand the freezing process in KLT1.8, we have simulated the dielectric permittivity for two different temperature dependencies of the mean relaxation time: a) $\tau_{mean} = \frac{C}{T-T_C}$, according to which the mean relaxation time diverges at the transition, and b)$\tau = A \exp \frac{-(T-T_{min})^2}{B}$, according to which it only reaches a maximum value at T_{min} and decreases below, as observed experimentally. Note that the first expression corresponds to the sudden or discontinuous freezing scenario described earlier, but the other is a hybrid scenario between discontinuous and continuous that starts with the freezing of a fraction of the PNDs, those with the longest relaxation times, and is followed by the progressive freezing of the remaining ones. Both expressions for the relaxation time were substituted into the Debye expression for ϵ' and the calculated permittivity curves are shown in Fig. 6 for different frequencies. Expression b) reproduces the observed temperature dependence of ϵ', exhibiting a double peak structure with a

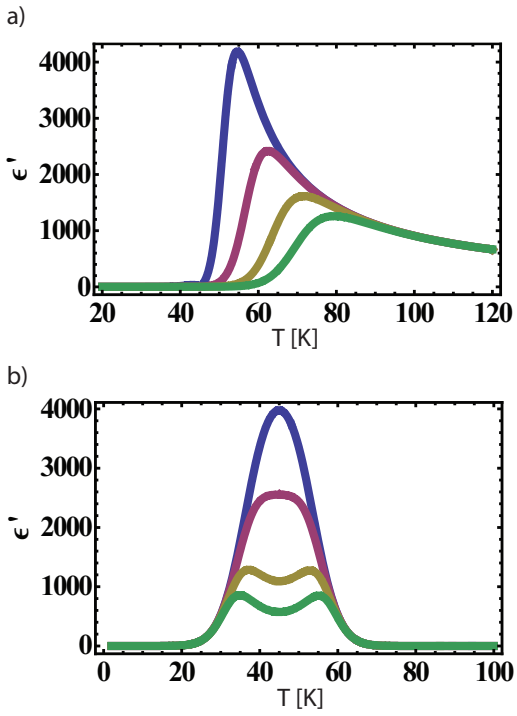

FIG. 6. (color online). Calculated frequency dependent dielectric response across the critical temperature T_c. (a) The typical relaxor behavior by assuming the average relaxation diverge as Curie-Weiss law. (b) Dispersion with an uniform minimum by assuming the average relaxation time increases to some finite value at T_{min} then slowly decreases.

minimum at T_{min} for higher frequencies and a single peak at the same temperature for lower frequencies. This simulation is clearly approximate in that it does not take into account the decreasing $\delta\epsilon$ below T_{min}. Such a decrease would introduce an asymmetry in the permittivity as is observed experimentally in Fig. 3.

The observation of a minimum in the dielectric permittivity has been reported before in hydrogen bonded molecular ferroelectric systems [23–26]. In these H-bonded systems, ferroelectricity is induced by the alignment of polar molecules that reside in each unit cell and have orientational degrees of freedom. A minimum is observed in their dielectric permittivity at the order-disorder transition and two distinct Curie constants, C_+ and C_-, are measured on either side of it. The permittivity minimum in these systems marks the occurrence of an equilibrium phase transition preceded by a critical slowing down of the orientational dynamics of the molecules. H-bonded ferroelectrics and KLT1.8 are similar in that both systems contain polar units with orientational degrees of freedom, which are correlated to one another independently of (or in parallel to) lattice correlations. Their main difference is that, in the molecular ferroelectrics, every unit cell is occupied by a molecule and a long range ferroelectric order is established below the transition while, in KLT1.8, the polar units (PNDs or isolated Li dipoles) are randomly distributed and do not interact as strongly with one another to induce a structural distortion. It is interesting to note that, because the orientational correlations between molecules are relatively independent of lattice correlations, H-bonded ferroelectrics can exhibit incommensurate phase transitions preceding their ferroelectric transition. Evidence for partial incommensurate transitions has also been reported in the context of relaxor ferroelectrics [34].

V. CONCLUSIONS

As illustrated by $K_{1-x}Li_xTaO_3$ (KLT) for two concentrations, $x = 0.018$ and $x = 0.026$, the collective dynamics and transition behavior of relaxors are very sensitive to composition in a certain critical range corresponding to the percolation of either polarization and/or strain through the system. Both KLT1.8 and KLT2.6 exhibit the relaxor behavior indicative of the presence of polar nanodomains (PNDs). But for Li concentrations just above the critical concentration of $x_c \approx 0.022$, KLT exhibits a first order structural transition marked by an abrupt drop in the dielectric permittivity. By contrast, for Li concentrations just below x_c, KLT exhibits a freezing transition, the onset of which is marked by a minimum in the dielectric permittivity for higher frequencies and a maximum for lower frequencies. Because both the minima at higher frequencies and the maxima at lower frequencies all appear at the same temperature, the freezing transition is a collective effect in which a fraction of the PNDs cease to relax. Above x_c, the mean relaxation time, τ_{mean} increases with decreasing temperature, exhibits a sharp discontinuity at the transition and resume its increase below the transition, as the orientation of the remaining dynamic PNDs grow progressively more constrained by the growing structural distortion. By contrast, below x_c, τ_{mean} evolves in a continuous manner, reaching a maximum at the freezing transition and decreasing below, due to the shorter relaxation times of the remaining dynamic PNDs, although their numbers progressively shrink. Hence, the transition behavior in KLT changes drastically upon crossing the critical concentration x_c. Such a drastic change in transition behavior across the critical concentration x_c may be attributed to the piezoelectric character of PNDs which ultimately drives the structural transition, a critical level of local polarization and therefore local strain being required to induce a macroscopic structural transformation. The critical concentration can thus be likened to the concentration at which the strain percolates through the system. This transition in low concentration KLT presents similarities with the glass or jamming transitions observed in glass and granular materials.

ACKNOWLEDGMENTS

We are grateful to P. Gehring (NCNR-NIST) and J. Gunton (Physics Dpt., Lehigh University) for stimulating discussions and to the NIST Center for Neutron Research for use of the facilities.

* Present address: Science and Technology Division, Corning Incorporated, Corning, NY, 14831

[1] G. Samara, J. Phys.: Condens. Matt. **15**, R367 (2003).

[2] R. Pattnaik, J. Toulouse, and B. George, Phys. Rev. B **62**, 12820 (2000).

[3] W. Kleemann, S. Kutz, and D. Rytz, Europhys. Lett. **4**, 239 (1987).

[4] J. Toulouse, B. E. Vugmeiste, and R. Pattnaik, Phys. Rev. Lett. **73**, 3467 (1994).

[5] U. Hochli and M. Maglione, J. Phys.: Condens. Matt. **1**, 2241 (1989).

[6] J. van der Klink, D. Rytz, F. Borsa, and U. Hochli, Phys. Rev. B **27**, 89 (1983).

[7] U. Hochli, H. Weibel, and L. Boatner, Phys. Rev. Lett. **41**, 1410 (1978).

[8] W. Kleemann, J. Dec, S. Miga, and D. Rytz, Z. Kristallogr. **226**, 145 (2011).

[9] V. Laguta, M. Glinchuk, and I. Kondakova, Phys. of the Solid State **46**, 1262 (2003).

[10] H. Yokota, A. Okada, I. Ishida, and Y. Uesu, Jpn. J. of App. Phys. **46**, 7167 (2007).

[11] A. Bokov and Z.-G. Ye, J. of Mat. Sci. **41**, 31 (2006).

[12] P. Debenedetti and F. Stillinger, Nature **410**, 259 (2001).

[13] J. Mauro, P. Gupta, and R. Loucks, J. of Chem. Phys. **126**, 184511 (2007).

[14] A. S. Keys, A. R. Abate, S. C. Glotzer, and D. J. Durian, Nature Phys. **3**, 260 (2007).

[15] G. Downing, G. Lamaze, and J. Langland, J. Res. Natl. Inst. Stand. Technol. **98**, 109 (1993).

[16] J. Robinson, *Design, Construction, and Characterization of a Neutron Depth Profiling Facility at the Oregon State University TRIGA® Reactor with an Advanced Digital Spectroscopy System*, Ph.D. thesis, Oregon State University (2012).

[17] S. Andrews, J.Phys.C: Solid State Phys. **18**, 1357 (1985).

[18] E. Courtens, J.Phys.C: Solid State Phys. **14**, L37 (1981).

[19] H. Yakota, Y. Uesu, C. Maliburt, and J. Kiat, Phys. Rev. B **75**, 184113 (2007).

[20] J. Toulouse, L. Cai, R. Pattnaik, and L. Boatner, Europhys. Lett. **105**, 17001 (2014).

[21] C. Stock, P. M. Gehring, G. Xu, D. Lamago, D. Reznik, M. Russina, J. Wen, and L. A. Boatner, Phys. Rev. B **90**, 224302 (2014).

[22] J. Wen, G. Xu, C. Stock, P. Gehring, Z. Zhong, L. Boatner, E. Venturini, and G. Samara, Phys. Rev. B **78**, 144202 (2008).

[23] E. Nakamura and M. Hosoya, J. of Phys. Soc. Jpn **23**, 844 (1967).

[24] A. Tamaki, T. Fujimura, and K. Kamiyoshi, J. of Chem. Phys. **65**, 4867 (1976).

[25] J. Baran, B. Bator, R. Jakubas, and M. Sledz, J. Phys.: Condens. Matter **8**, 10647 (1996).

[26] A. Piecha and R. Jakubas, J. Phys.: Condens. Matter **21**, 015904 (2009).

[27] S. Prosandeev, E. Cockayne, and B. Burton, Phys. Rev. B **68**, 014120 (2003).

[28] G. Geneste, J.-M. Kiat, H. Yokota, Y. Uesu, and F. Porcher, Phys. Rev. B **81**, 144112 (2010).

[29] J. Dec, S. Miga, Z. Trybula, K. Kaszynska, and W. Kleemann, J. of Appl. Phys. **107**, 094102 (2010).

[30] S. Prosandeev, L. J. V.A. Trepakov, M.E. Savinov, and S. Kapphan, J. Phys.: Condens. Matter **13**, 9749 (2001).

[31] K. S.Cole and R. H.Cole, J. of Chem. Phys. **9**, 341 (1941).

[32] T. S. Majmudar, M. Sperl, S. Luding, and R. P. Behringer, Phys. Rev. Lett. **98**, 058001 (2007).

[33] P. Chaudhuri, L. Berthier, and S. Sastry, Phys. Rev. Lett. **104**, 165701 (2010).

[34] C. Randall, A. Bhalla, T. Shrout, and L. E. Cross, J. Mater. Res. **5**, 829 (1990).